

Up- and Down-Conversion Cubic Zirconia and Hafnia Nanobelts**

By Changlong Jiang, Feng Wang, Nianqiang Wu,* and Xiaogang Liu*

One-dimensional (1D) metal oxide nanomaterials, such as zinc oxide (ZnO) nanowires and nanobelts (or nanoribbons), have recently attracted immense attention due to their size- and shape-dependent optical, mechanical, and electronic properties.^[1] In stark contrast, investigations of 1D zirconia (ZrO₂) and hafnia (HfO₂) nanomaterials remain unexploited largely because of the formidable challenges associated with the fabrication of these structures with controlled dimensions and crystal phases. ZrO₂ and HfO₂ materials typically exhibit three primary polymorphs (monoclinic, tetragonal, and cubic) and have important technological applications as catalyst supports,^[2] oxygen detectors,^[3] high-temperature fuel cell electrolytes,^[4] gate dielectric in metal-oxide semiconductor devices,^[5] and optical waveguides.^[6] Apart from a few rare examples of rod-like polycrystalline structures formed via porous alumina templates or by using an inverse microemulsion technique, most of the ZrO₂ nanomaterials obtained thus far are best classified as nanoparticles and thin films.^[7] Here, we introduce a direct and scalable approach, based upon a thermal decomposition method under normal atmospheric pressure, for growing well-defined single-crystalline cubic ZrO₂ and HfO₂ nanobelts with controllable structural compositions and novel optical properties. To the best of our knowledge, these nanomaterials provide the first evidence of ZrO₂ and HfO₂ crystals with belt-like morphology.

In a typical synthesis of the ZrO₂ precursors, a solution of ZrCl₄ (1.6 g, 7 mmol) and YCl₃·6H₂O (0.3 g, 1 mmol) in ethanol (10 mL) was first treated with sodium hydroxide (1.5 g, 38 mmol) to yield a viscous gel mixture. The mixture was transferred into a 15 mL Teflon-lined autoclave and heated at 140 °C for 24 h. Upon cooling the resulting precipitate was

collected by filtration, washed with distilled water several times, and further dried at 50 °C to yield ZrO₂ precursors. The as-synthesized ZrO₂ precursors are composed of Zr(OH)₄ as characterized by Fourier transform (FT)-IR and thermal analysis (Fig. S1 and S4 of Supporting Information). The precursors were then placed on a silicon substrate (10 mm × 10 mm × 1 mm) and transferred into an alumina boat (70 mm × 14 mm × 10 mm). The alumina boat was heated in a furnace to 700 °C at a rate of 2 °C min⁻¹ and subsequently annealed at 700 °C for 90 min under atmospheric pressure. A scanning electron microscopy (SEM) image of a typical yttria-stabilized zirconia (YSZ) product (Fig. 1A) obtained after thermal treatment shows primarily belt-like structures with a lateral size ranging from 200 to 500 nm and length of several tens of micrometers. The width disparity is largely due to the inhomogeneous sizes of the Zr(OH)₄ particles. Figure 1B shows the high-magnification SEM image of a typical single YSZ nanobelt with remarkably smooth surface morphology and a thickness of ~15 nm. The crystalline phase of the YSZ nanobelts was determined by X-ray powder diffraction (XRD). All peaks in Fig. 1C can be indexed to face-centered cubic ZrO₂ (Joint Committee on Powder Diffraction Standards (JCPDS) card no. 49-1642). We attribute the stable cubic ZrO₂ phase at room temperature to the replacement of quadrivalent Zr by trivalent Y (12.5 mol %), which leads to a high concentration of structural oxygen vacancies for charge compensation and stabilizes the cubic phase (inset, Fig. 1C). In contrast, XRD patterns of the YSZ samples obtained with less Y³⁺ content (0, 4, and 9 mol %) show a mixture of monoclinic, tetragonal, and cubic phases (Fig. S2 of Supporting Information). Transmission electron microscopy (TEM) images recorded on individual nanobelts (Fig. 2A and B) provide further insight into the structure of these materials. Figure 2A clearly shows belt-like structures of the YSZ nanomaterials. Energy-dispersive X-ray analysis of individual nanobelts shows that they contain Y, Zr, and O (Fig. 2B). The high-resolution TEM image of a single-crystalline YSZ nanobelt shows an atomically flat edge with a spacing of 0.30 nm between adjacent lattice planes that corresponds to the distance of two (111) crystal planes, proving <111> to be the preferred growth direction for the YSZ nanobelts (Fig. 2C).

In a further set of experiments, we studied temperature profiles for the formation of cubic YSZ nanobelts. XRD patterns of the precursors of ZrO₂ calcinated at various temperatures are shown in Figure S3 (Supporting Informa-

[*] Prof. X. Liu, Dr. C. Jiang, Dr. F. Wang
Department of Chemistry, National University of Singapore
3 Science Drive 3, Singapore 117543 (Singapore)
E-mail: chmlx@nus.edu.sg

Prof. N. Wu
Department of Mechanical and Aerospace Engineering
West Virginia University, Morgantown, WV 36506 (USA)
E-mail: nick.wu@mail.wvu.edu

[**] This study was supported by NUS Academic Research Fund (grant nos. R-143-000-317 and R-143-000-342) and a Young Investigator Award (grant no. R-143-000-318) to X. L. by NUS. N. W. acknowledges the partial financial support of WV Nano Nanoscience Initiative Fund through the West Virginia University Research Corporation. X. L. is grateful to Y. Han for helpful discussions. Supporting Information is available online from Wiley InterScience or from the author.

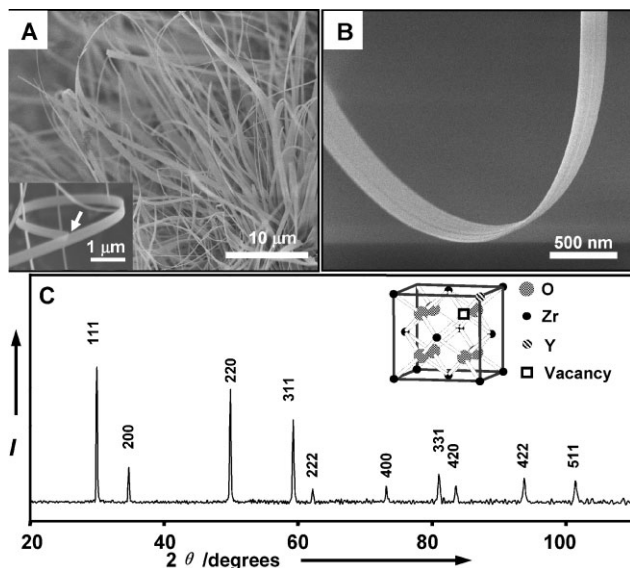


Figure 1. A) SEM image of the YSZ nanobelts (inset: SEM image showing the rectangular end of a nanobelt marked by an arrow). B) High-resolution SEM image showing the cross-section of a single nanobelt. C) XRD patterns of the YSZ nanobelts (inset: a representative fcc unit cell of YSZ crystals).

tion). At 200 °C the sample shows absence of any crystalline phase, while at 300 °C small peaks start developing, suggesting the formation of a crystalline phase. At 400 °C a mixture of monoclinic and cubic phases is clearly visible, and the cubic phase becomes predominant at 500 °C. A further increase in temperature induces a complete phase transformation from monoclinic to cubic phase. The XRD results are also consistent with thermogravimetry and differential thermal analysis (TG-DTA, Fig. S4 of Supporting Information). In addition,

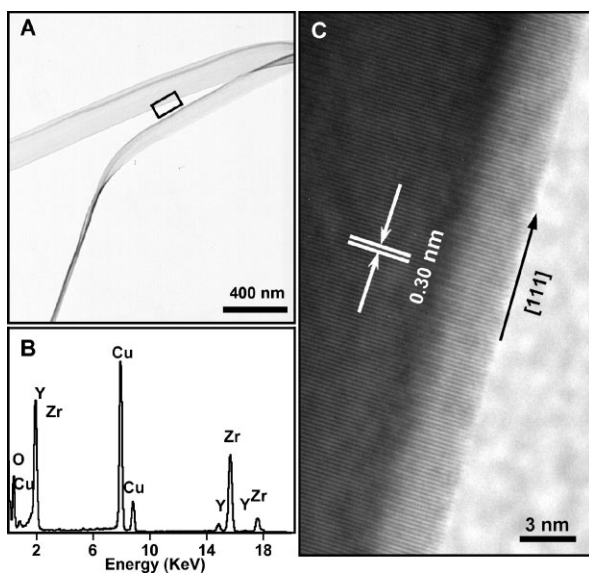


Figure 2. A) TEM image of the YSZ nanobelts. B) EDX patterns of the nanobelts. Note that the strong signals for Cu come from the copper TEM grid. C) HRTEM showing the lattice fringes of a nanobelt marked in (A).

our SEM study reveals that the YSZ nanobelts start growing at around 550 °C (Fig. 3). As the temperature increases, the coverage of the nanobelt array on the substrate becomes uniform. The widths of these nanobelts can be controlled by adjusting the heating rate. A slow heating rate typically leads to the formation of nanobelts with increased lateral dimension (Fig. 3E).

The formation of cubic YSZ nanobelts can be attributed to thermal decomposition of the zirconia precursors and a subsequent diffusion-growth mechanism (Scheme 1). Upon heat treatment, the $Zr(OH)_4$ microparticles undergo dehydration and decomposition, to form ZrO_2 followed by the phase transition from monoclinic to cubic phase. As the decomposition starts, a thin layer of ZrO_2 that forms on the surface of the $Zr(OH)_4$ particles will result in substantial stress at the $ZrO_2/Zr(OH)_4$ interface because of their structural and density differences. The accumulation of the stress subsequently leads to dislocations in the ZrO_2 crystals, accompanied by atom diffusion in the preferred growth direction along $\langle 111 \rangle$ and the formation of the nanobelts. In addition, the thinning of the nanobelt tips is largely attributed to more difficulty in the long-range diffusion along the longitudinal direction as compared to the lateral direction. Cubic HfO_2 nanobelts can also be synthesized by this method because of similar structural characteristics of the ZrO_2 and HfO_2 materials (Fig. S5 of Supporting Information).

Importantly, unlike ZnO, nanocrystalline ZrO_2 and HfO_2 materials provide excellent platforms for the incorporation of a broad range of rare-earth ions, due to their close lattice match to Zr and Hf,^[6] thus offering unique optical properties because of the abundant f-f electronic transitions of the dopant ions. In addition to YSZ, we have synthesized cubic ZrO_2 nanobelts doped with Ce^{3+} or Er^{3+} . For example, Er^{3+} -doped nanobelts

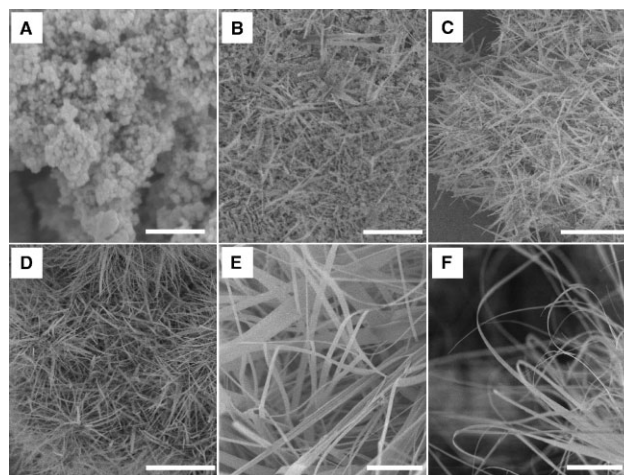
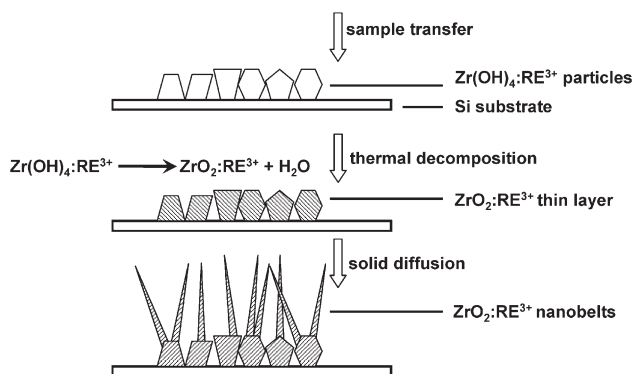


Figure 3. SEM images of the cubic ZrO_2 samples (doped with 12.5 mol % YCl_3) synthesized at different heating temperatures and heating rates. A) without heating, B) at 550 °C with a heating rate of 2 °C min^{-1} , C) at 600 °C with a heating rate of 2 °C min^{-1} , D) at 650 °C with a heating rate of 2 °C min^{-1} , E) at 700 °C with a heating rate of 1 °C min^{-1} , and F) 700 °C with a heating rate of 2 °C min^{-1} (scale bars are 5 μm).



Scheme 1. A schematic illustration of rare-earth (RE)-doped nanobelt growth.

show a dual capability for both down- and up-conversion emissions in the visible range (Fig. 4). The down-conversion emission (excited at 280 nm) spectrum that is independent of dopant ions shows a peak centered at 470 nm, corresponding to band gap emission of the host (Fig. 4A).^[8] In the up-conversion spectrum (excited at 980 nm), characteristic emission patterns can be observed and assigned to ${}^2\text{H}_{11/2} + {}^4\text{S}_{3/2} \rightarrow {}^4\text{I}_{15/2}$ (515–565 nm) and ${}^4\text{F}_{9/2} \rightarrow {}^4\text{I}_{15/2}$ (640–690 nm) transitions of Er^{3+} , respectively (Fig. 4B).^[9]

In conclusion, we have demonstrated that a thermal decomposition route can be used for the synthesis of single-crystalline cubic ZrO_2 and HfO_2 nanobelts under atmospheric pressure. The dopant concentrations and heat-treatment process enable growth of the nanobelts with controlled feature shape, dimension and crystal phase. These novel ZrO_2 and HfO_2 nanobelts should represent well-defined nanoscale structures or building blocks needed both for fundamental optical studies (e.g., multicolor emission tuning^[10]) and for the development of integrated photonic devices and oxygen sensors.

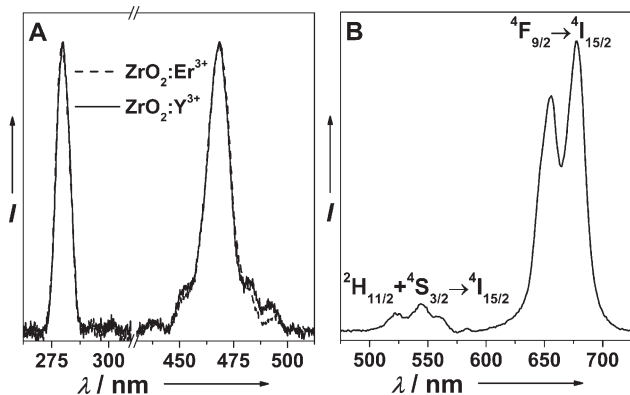


Figure 4. A) Room-temperature down-conversion excitation (left) and emission (right) spectra of ZrO_2/Y (12.5 mol %) and ZrO_2/Er (12.5 mol %) nanobelts. B) The corresponding up-conversion emission spectrum of the ZrO_2/Er nanobelts. The sample was excited at 980 nm with a 600 mW diode laser.

Experimental

Chemicals: ZrCl_4 (99.9%), HfCl_4 (99.9%), NaOH , $\text{YCl}_3 \cdot 6\text{H}_2\text{O}$ (99.99%), $\text{CeCl}_3 \cdot 7\text{H}_2\text{O}$ (99.9%), and $\text{ErCl}_3 \cdot 6\text{H}_2\text{O}$ (99.9%) were purchased from Sigma–Aldrich and used as starting materials without further purification.

Characterization: SEM images were recorded by field-emission scanning electron microscopy (JEOL 6701). TEM measurements were carried out on a JEOL 3010 transmission electron microscope operating at an acceleration voltage of 300 kV. The crystallographic phase of the sample was determined by powder XRD on a Siemens D5005 X-ray diffractometer with $\text{CuK}\alpha$ radiation ($\lambda = 1.5406 \text{ \AA}$) at a scan rate of 0.01 degrees per second. Thermogravimetric analysis was performed on a SDT 2960 TGA thermal analyzer with a heating rate of $10^\circ\text{C min}^{-1}$ in air using a sample size of about 20 mg per run. The luminescence spectra were obtained with a DM150i monochromator equipped with a R928 photon counting photomultiplier tube (PMT), in conjunction with a 980 nm diode laser and a 180 W xenon lamp.

Received: May 28, 2008

Published online: October 20, 2008

- [1] a) Y. Xia, P. Yang, Y. Sun, Y. Wu, B. Mayers, B. Gates, Y. Yin, F. Kim, H. Yan, *Adv. Mater.* **2003**, *15*, 353. b) Y. Wang, X. Jiang, Y. Xia, *J. Am. Chem. Soc.* **2003**, *125*, 16176. c) Y. Cui, C. M. Lieber, *Science* **2001**, *291*, 851. d) Z. Pan, Z. Dai, Z. L. Wang, *Science* **2001**, *291*, 1947. e) M. Huang, S. Mao, H. Feick, H. Yan, Y. Wu, H. Kind, E. Weber, R. Russo, P. Yang, *Science* **2001**, *292*, 1897. f) J. Xu, N. Wu, C. Jiang, M. Zhao, J. Li, Y. Wei, S. X. Mao, *Small* **2006**, *2*, 1458. g) X. Wang, J. Song, J. Liu, Z. L. Wang, *Science* **2007**, *316*, 102. h) J. Liu, Q. Li, T. Wang, D. Yu, Y. Li, *Angew. Chem.* **2004**, *116*, 5158. *Angew. Chem. Int. Ed. Engl.* **2004**, *43*, 5048. i) S. Myung, M. Lee, G. T. Kim, J. S. Ha, S. Hong, *Adv. Mater.* **2005**, *17*, 2361. j) T. Xu, J. Zheng, N. Wu, A. W. Nicholls, J. R. Roth, D. A. Dikin, R. S. Ruoff, *Nano Lett.* **2004**, *4*, 963. k) C. Klingshirn, *Phys. Status Solidi B* **2007**, *244*, 3027. l) Z. R. Tian, J. A. Voigt, J. Liu, B. Mckenzie, M. J. Mcdermott, M. A. Rodriguez, H. Konishi, H. Xu, *Nature Mater.* **2003**, *2*, 821. m) T. Zhang, W. Dong, M. Keeter-Brewer, S. Konar, R. N. Njabon, Z. R. Tian, *J. Am. Chem. Soc.* **2006**, *128*, 10960. n) B. S. Guiton, Q. Gu, A. L. Prieto, M. S. Gudiksen, H. Park, *J. Am. Chem. Soc.* **2005**, *127*, 498. o) J. Yuan, J. Laubernds, S. Villegas, S. Gomez, S. L. Suib, *Adv. Mater.* **2004**, *16*, 1729. p) C. Liu, J. Zapien, Y. Yao, X. Meng, C. Lee, S. Fan, Y. Lifshitz, S.-T. Lee, *Adv. Mater.* **2003**, *15*, 838. q) S. Mathur, S. Barth, *Small* **2007**, *3*, 2070. r) S. Mathur, S. Barth, U. Werner, F. Hernandez-Ramirez, *Adv. Mater.* **2008**, *20*, 1550. s) J. Yuan, X. Liu, O. Akbulut, J. Hu, S. L. Suib, J. Kong, F. Stellacci, *Nature Nano.* **2008**, *3*, 332.
- [2] M. Hino, K. Arata, *Chem. Commun.* **1988**, 1259.
- [3] G.-L. Tan, X.-J. Wu, *Thin Solid Films* **1998**, *330*, 59.
- [4] U. Brossmann, R. Würschum, U. Södervall, H.-E. Schaefer, *J. Appl. Phys.* **1999**, *85*, 7646.
- [5] Y. Lu, S. Bangsaruntip, X. Wang, L. Zhang, Y. Nishi, H. Dai, *J. Am. Chem. Soc.* **2006**, *128*, 3518.
- [6] A. Patra, C. S. Friend, R. Kapoor, P. N. Prasad, *J. Phys. Chem. B* **2002**, *106*, 1909.
- [7] a) H. Cao, X. Qiu, B. Luo, Y. Liang, Y. Zhang, R. Tan, M. Zhao, Q. Zhu, *Adv. Funct. Mater.* **2004**, *14*, 243. b) Y. Liu, C. Zheng, W. Wang, Y. Zhan, G. Wang, *J. Am. Ceram. Soc.* **2002**, *85*, 3120. c) M. Copel, M. Gribelyuk, E. Gusev, *Appl. Phys. Lett.* **2000**, *76*, 436.
- [8] E. De la Rosa-Cruz, L. A. Diaz-Torres, P. Salas, R. A. Rodriguez, G. A. Kumar, M. A. Meneses, J. F. Mosino, J. M. Hernandez, O. Barbosa-Garcia, *J. Appl. Phys.* **2003**, *94*, 3509.
- [9] a) G. Blasse, B. C. Grabmaier, *Luminescent Materials*, Springer-Verlag, Berlin **1994**. b) F. Auzel, *Lumines. Rev.* **2004**, *104*, 139. c) S. Heer, K. Kömpe, H.-U. Güdel, M. Haase, *Adv. Mater.* **2004**, *16*, 2102. d) G.

- Yi, H. Lu, S. Zhao, G. Yue, W. Yang, D. Chen, L. Guo, *Nano Lett.* **2004**, *4*, 2191. e) J. Zeng, J. Su, Z. Li, R. Yan, Y. Li, *Adv. Mater.* **2005**, *17*, 2119. f) S. Sivakumar, F. C. J. M. van Veggel, M. Raudsepp, *J. Am. Chem. Soc.* **2005**, *127*, 12464. g) J. C. Boyer, F. Vetrone, L. A. Cuccia, J. A. Capobianco, *J. Am. Chem. Soc.* **2006**, *128*, 7444. h) D. K. Chatterjee, A. J. Rufaihah, Y. Zhang, *Biomater.* **2008**, *29*, 937.
- [10] a) F. Wang, X. Xue, X. Liu, *Angew. Chem.* **2008**, *120*, 920; *Angew. Chem. Int. Ed.* **2008**, *47*, 906. b) F. Wang, X. Liu, *J. Am. Chem. Soc.* **2008**, *130*, 5642.